Melting temperature effects on the size of ion-induced craters

K. Nordlund, K. O. E. Henriksson and J. Keinonen

Accelerator Laboratory, P.O. Box 43, FIN-00014 University of Helsinki, Finland

(September 8, 2001)

Recent work on the sizes of craters produced by ion impacts of solids has shown that the size of the crater scales with the inverse square of the cohesive energy. This observation is in contrast to the size of craters produced in macroscopic impacts, which scale directly with the inverse of the cohesive energy. It has relied on the assumption that the melting temperature is proportional to the cohesive energy. Using computer simulations, we now show that the size scales in fact with the inverse of the product of the melting temperature and cohesive energy. This provides direct proof that the reason to the different behavior of macroscopic and ion-induced cratering is flow of the liquid produced by the ions.

The production of craters has been observed in a wide range of systems in nature, ranging from craters produced by meteor impacts on planets and gas guns on solids to those produced by ion impacts on metals and insulators[1–5]. Analysis of the crater size and shapes have shown that several of the scaling laws used in describing their behavior apply both to the macroscopic and microscopic (ion-induced) regimes. However, one of the central laws, the one which describes the dependence on the crater size on the cohesive energy E_{coh} of the material, differs in the two regimes[6]. For the macroscopic craters, the crater size N_{cr} (measured e.g. by the volume of the excavated region) scales as

$$N_{cr} \propto \frac{1}{E_{coh}} \tag{1}$$

whereas for the microscopic craters the behavior

$$N_{cr} \propto \frac{1}{E_{coh}^2} \tag{2}$$

has been reported[6,7].

The latter scaling behavior is observed when the cohesive energy of a material is modified in a computer simulation by simply scaling the depth of the potential well[6,8]. In this kind of a modification, the melting temperature will scale directly with the cohesive energy[9]. Although this choice of scaling is a natural choice, it does not allow for distinguishing between melting point and cohesive energy effects. Being able to do this would be interesting because it has been assumed, without direct proof, that the difference between the macroscopic and microscopic behavior is due to the liquid flow made possible by the intense heat generated by ion impacts[6,10].

In a previous work, we have found that in atomistic computer simulations it is quite possible to modify the melting point of a material without any effect on the cohesive energy or other equilibrium properties[11]. In that work, we constructed two different potential models for Pd on one hand, and Pt on the other, to test the effect of the melting point on ion beam mixing. We will here utilize these potential models to compare cratering in the same material under identical conditions for each impact energy, so that the only difference is the melting point.

In practice, we used clusters of 13 atoms for producing craters since previous work has shown that the fluctuations in crater size are reduced with the increasing cluster size[12].

The principles of our MD simulations have been discussed in other papers[11,13,14], so here we review only the features most relevant for the present work. In order to have a surface, periodic boundary conditions are switched off in one direction, in the one defining the z direction. To describe the heat conduction into the medium, all borders except the surface are damped, that is, three atom layers at the borders are kept at a temperature of 0 K using Berendsen's temperature control method[15].

In this work, each cluster had icosahedral symmetry, having one center atom and 12 nearest neighbors, due to the face-centered cubic (fcc) lattice. The cluster was rotated with a random polar and azimuthal angle, and translated a random distance a_x and a_y in the x and y directions, respectively. Here $a_x, a_y \in [-a_0/2, a_0/2]$, a_0 being the lattice parameter. These rotation and translation operations introduced an element of randomness into each simulation, as required to generate statistics.

The cluster, which always consisted of the same atom type as those in the bulk, was positioned outside the potential cutoff (~ 5 Å) of the nearest bulk atom. In order to start the cluster moving against the bulk surface, a kinetic energy of $E_0/13$ was given to the atoms in the cluster.

The incident atoms lose energy in elastic collisions with the bulk atoms (nuclear stopping), and also by inelastic collisions with the electrons (electronic stopping). In the simulations the electronic stopping[16,17] was applied to all atoms having a kinetic energy of at least 5 eV.

A potential based on the embedded atom method by Foiles[18] was used to describe equilibrium properties. We used both the original potential, and a modified version which was designed to keep the equilibrium properties unchanged, but give a better description of the melting point than the original potential[11]. We obtained the latter potential by modifying the potential with a function $f(r) = -a(r - r_i) + 1$ when $r < r_i$. When $r \geq r_i$ we had $f(r) = 1$. The value of r_i was chosen to be less than the equilibrium nearest-neighbour distance to ensure that the equilibrium properties are

unaffected. We chose the parameters r_i and a to obtain a good reproduction of both the melting point and threshold displacement energy. At close separations all the EAM potentials were smoothly joined to the universal Ziegler-Biersack-Littmark interatomic repulsive potential[16] to realistically describe strong collisions. The original potentials, denoted by Pt-A and Pd-A, had melting temperatures of 1530 ± 20 K and 1415 ± 5 K, respectively. The modified potentials, denoted by Pt-B and Pd-B, had melting temperatures of 2130 ± 10 K and 1910 ± 20 K, respectively. The potentials were also found to be in good agreement with experimental high-pressure equation of state[19,20] data in the pressure regime below 100 GPa relevant in collision cascades[21].

The development of the cluster hitting the bulk surface, the resulting (displacement) cascade, the formation of a microscopic explosion accompanied with liquid flow and eventually the cooling down of the system was followed for 50 ps, in all the cases of cluster energy. This time was enough to cool down the system and achieve a stable crater, as determined by visual inspection.

As a rule, 14 simulations were carried out for each kind of cluster impinging on the surface of the bulk. Half of these used the modified potential. For example, in the case of 20 keV Pt_{13} clusters impinging on Pt and using the potential denoted by Pt-A, 7 simulations were carried out. However, in the case of self-bombardment of Pt by 2 keV clusters, results where gathered from a total of 60 simulations in order to obtain enough statistics.

In all the simulations, the uncertainty in N_{cr} was at most 18.4 % (Pt-B in the case of 2 keV clusters) and at least 3.5 % (Pt-B in the case of 40 keV clusters).

TABLE I. Crater sizes in the form of number of excavated atoms and crater radii.

Model	Energy (keV)	N_{cr}	R_{cr} (Å)
Pt-A	2	111 ± 17	9.8 ± 0.6
	20	1665 ± 61	24.9 ± 0.6
	40	3398 ± 265	32.9 ± 0.7
Pd-A	20	1971 ± 80	25.9 ± 0.5
Pt-B	2	67 ± 12	7.8 ± 0.7
	20	1112 ± 68	21.3 ± 1.0
	40	2372 ± 84	27.9 ± 0.7
Pd-B	20	1382 ± 89	23.4 ± 3.4

Crater sizes in the form of number of excavated atoms and crater radius are presented in table I. N_{cr} is simply the sum of the number of sputtered atoms and adatoms, $N_{cr} = N_{sput} + N_{ad}$. This practically equals the number of excavated atoms, since there are almost no defects outside the crater itself.

The crater radius R_{cr} is derived from the expression $N_{su}/n = A = \pi R_{cr}^2$, where n is the areal density of atoms of the topmost bulk atom layer and N_{su} is the number of missing atoms in the topmost bulk atom layer due to the presence of the crater. The expression is inspired by the roughly circular appearance of the crater wells in the cascade simulations initiated by 20 and 40 keV clusters.
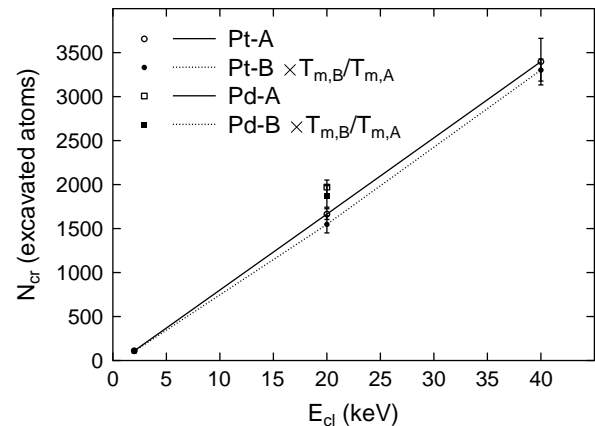
a)
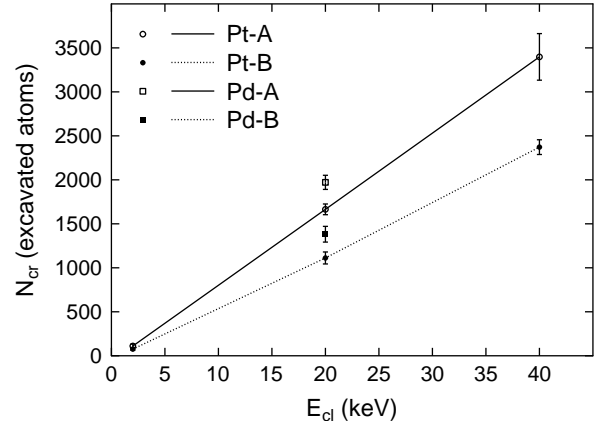
b)

FIG. 1. a) Crater size N_{cr} as a function of the kinetic energy E_{cl} of the bombarding cluster. Pt-A and Pd-A are the original Foiles interatomic potentials[18], Pt-B and Pd-B the models where the melting point has been modified to be close to the experimental value[11]. b) is as a), but here the results for potentials Pt-B and Pd-B are multiplied by the ratio $T_{melt,B}/T_{melt,A}$ where $T_{melt,x}$ is the melting point for model x, with x equal to A or B.

The crater size N_{cr} for the simulated cases is illustrated in Fig. 1 a). Clear differences are obtained in the crater sizes. Since for each material the cohesive energy is exactly the same for the two models used, the crater size does not depend on the cohesive energy alone. In Fig. 1 a) we plot the same data, but now scaling the data for models Pt-B and Pd-B with the ratio $T_{melt,B}/T_{melt,A}$. Now the crater sizes agree within the uncertainties. Bearing in mind that this result still has to be consistent with the previously observed dependence (Eq. 2) for the simpler (i.e. $T_{melt} \propto E_{coh}$) modification of a potential, our new result shows that the best way to describe the crater size dependence on material properties is

$$N_{cr} \propto \frac{1}{E_{coh} T_{melt}}. \tag{3}$$

A more detailed analysis, considering a generalized form for the scaling

$$N_{cr} \propto \frac{1}{E_{coh}T_{melt}^{1+x}}. \tag{4}$$

gave an upper limit $|x| \lesssim 0.2$ considering the uncertainties of the data.

The scaling behavior observed here can be understood by recalling that one factor of $1/E_{coh}$ is observed for macroscopic cratering, where melting usually plays no role. Our observation of another factor T_{melt} (rather than E_{coh}) in the denominator for microscopic cratering is a direct proof for the assumption that the difference between the two regimes is due to liquid flow. We emphasize that in our modification of the potential[11] all other quantities which could be expected to be relevant here, such as the elastic and heat conduction properties, are still unmodified. Hence the crucial additional parameter is better described as the melting point rather than any of the other quantities.

It is interesting to note that at 2 keV, the crater size still scales with the inverse of the melting point within the uncertainties, even though no long-lived heat spike can form at this low energy.

In conclusion, we have shown that the size of craters produced by energetic ion and cluster ion impact scales with the inverse of the product of the melting temperature and cohesive energy when other material parameters are the same. This proves that the difference between the crater production mechanisms for macroscopic and microscopic crater impacts is due to liquid flow in the latter case.

[1] G. Neukum and B. A. Ivanov, in *Hazards due to comets & asteroids*, *Space Science*, edited by T. Gehrels (The University of Arizona Press, Tucson, Arizona, 1994), p. 359.

[2] R. M. Schmidt and K. R. Housen, Intl. J. Impact Eng. **5**, 543 (1987).

[3] S. E. Donnelly and R. C. Birtcher, Phys. Rev. B **56**, 13599 (1997).

[4] R. M. Papaléo, L. D. de Oliveira, L. S. Farenzana, M. A. de Araújo, and R. P. Livi, Phys. Rev. B (Brief reports) **62**, 11273 (2000).

[5] K. Nordlund, Physics World **14**, 22 (2001).

[6] R. Aderjan and H. M. Urbassek, Nucl. Instr. Meth. Phys. Res. B **164-165**, 697 (2000).

[7] E. M. Bringa, R. Papaleo, and R. E. Johnson, (2001), submitted for publication.

[8] In an interatomic potential of the embedding-atom method type, this kind of scaling is achieved by multiplying both the pair potential and embedding energy parts with the same factor.

[9] E. Bringa, K. Nordlund, and J. Keinonen, Phys. Rev. B (2001), submitted for publication.

[10] M. Ghaly and R. S. Averback, Phys. Rev. Lett. **72**, 364 (1994).

[11] K. Nordlund, L. Wei, Y. Zhong, and R. S. Averback, Phys. Rev. B (Rapid Comm.) **57**, 13965 (1998).

[12] T. J. Colla, R. Aderjan, R. Kissel, and H. M. Urbassek, Phys. Rev. B **62**, 8487 (2000).

[13] K. Nordlund, M. Ghaly, R. S. Averback, M. Caturla, T. Diaz de la Rubia, and J. Tarus, Phys. Rev. B **57**, 7556 (1998).

[14] M. Ghaly, K. Nordlund, and R. S. Averback, Phil. Mag. A **79**, 795 (1999).

[15] H. J. C. Berendsen, J. P. M. Postma, W. F. van Gunsteren, A. DiNola, and J. R. Haak, J. Chem. Phys. **81**, 3684 (1984).

[16] J. F. Ziegler, J. P. Biersack, and U. Littmark, *The Stopping and Range of Ions in Matter* (Pergamon, New York, 1985).

[17] J. F. Ziegler, 1996, SRIM-96 computer code, private communication.

[18] S. M. Foiles, M. I. Baskes, and M. S. Daw, Phys. Rev. B **33**, 7983 (1986).

[19] H. K. Mao, P. M. Bell, J. W. Shaner, and D. J. Steinberg, J. Appl. Phys. **49**, 3276 (1978).

[20] V. N. Antonov, V. Y. Milman, V. V. Nemoshkalenko, and A. V. Zhalko-Titarenko, Z. Phys. B - Condensed Matter **79**, 233 (1990).

[21] R. S. Averback, J. Nucl. Mat. **216**, 49 (1994).